Journal of Materials Chemistry B

Accepted Manuscript

ROYAL SOCIETY OF CHEMISTRY

www.rsc.org/materialsB

Journal of Materials Chemistry B

Dynamic Article Links ►

Cite this: DOI: 10.1039/c0xx00000x

www.rsc.org/xxxxxx

ARTICLE

PCL microspheres tailored with carboxylated poly(glycidyl methacrylate)-REDV conjugates as conducive microcarriers for endothelial cell expansion

Shaojun Yuan,[a,#,*] Gordon Xiong,[b,#] Fei He,[a] Wei Jiang,[a] Bin Liang,[a] Simo Pehkonen,[c] Cleo Choong[b,*]

Received (in XXX, XXX) Xth XXXXXXXXX 2015, Accepted Xth XXXXXXXXX 20XX
DOI: 10.1039/b000000x

Microcarrier cell culture systems provide one of the most promising techniques for cell amplification due to their high surface area-to-volume ratio. In this study, biodegradable polycaprolactone (PCL) microspheres tethered with carboxylated poly(glycidyl methacrylate)-REDV conjugates were developed by the combination of surface-initiated atom transfer radical polymerization (ATRP) and azide-alkyne click chemistry as conducive microcarriers for rapid cell expansion of human umbilical vein endothelial cells (HUVECs). Azido-terminated poly(glycidyl methacrylate) (PGMA-N_3) brushes were grafted onto the PCL microspheres by surface-initiated ATRP. Subsequent carboxylation of PGMA-N_3 brushes was accomplished by azide-alkyne click reaction with hexynoic acid. REDV peptides were covalently conjugated to the pendent carboxyl groups on the side chain of carboxylated PGMA-COOH brushes via carbodiimide chemistry to enhance cytocompatibility of the three-dimension (3D) PCL scaffolding system. Success in each functionalization step was ascertained by the measurement of attenuated total reflectance-Fourier transform infrared spectroscopy (ATR-FTIR), *X*-ray photoelectron spectroscopy (XPS), scanning electron microscopy (SEM) and wet laser particle size analyzer. *In vitro* cell-loading assay of HUVECs demonstrated a significant improvement of cell adhesion and proliferation on the REDV-immobilized PCL microsphere surfaces, and a confluent layer of HUVECs were formed after 7 days of incubation. The highly biocompatible and transportable nature of functionalized PCL microcarriers offers a significant potential as a cell expansion platform.

1. Introduction

The seeding of endothelial cells onto synthetic materials[1, 2] and decellularized vascular tissue matrix[3-5] has gained attraction in the research area of tissue-engineered vascular grafts (TEVG) in recent years. The use of seeded TEVGs is purported to be able to meet current shortcomings in the use of native autologous vessels for bypass procedures, namely the lack of healthy or suitable vascular tissues in certain patients.[6, 7] An endothelium lining on the graft luminal surface is generally considered to be vital for maintaining a non-thrombogenic surface essential for reducing thrombosis after implantation.[8-10] In conjunction with the development of graft surfaces for supporting endothelial cell growth, bioreactors and pulsatile flow systems have been developed by many researchers to pre-endothelialize the graft surface or decellularized constructs *in vitro*.[11-13] Though *in vitro* endothelialization can be a promising approach for the development of TEVGs, it has to be accompanied by the availability of endothelial cells, usually obtained in small numbers from superficial vein biopsies,[14, 15] for any chance of clinical success. Studies have shown that low-density seeding of endothelial cells onto graft surfaces did not improve graft patency, due to a large proportion of endothelial cells lost to pulsatile blood flow; hence, a high density of endothelial cells was required to overcome this problem.[16] Thus, these developments in vascular engineering have given rise to a foreseeable need for the rapid scaling-up and expansion of viable endothelial cells from patients, which is an area seldom addressed by researchers in the field.

Microcarriers have been used in industrial-scale bioreactors for the growth and expansion of various cell types for other tissue engineering applications. First used to cultivate mammalian cell lines for large-scale vaccine production,[17] microcarriers have been explored extensively for the culture of embryonic stem cells,[18] mesenchymal stem cells,[19-21] osteoblasts,[22] chondrocytes,[23] and hepatocytes.[24, 25] Microcarriers have also been used successfully as cell delivery systems to regenerate lost tissues, either applied directly via injection.[24] or incorporation into tissue engineered scaffolds to be implanted at defective tissue sites.[26] The various materials that microcarriers have been manufactured from include

Electronic Supplementary Information (ESI) available: See DOI:10.1039/b000000x/

# These authors contributed equally.
[a]*Multiphase Mass Transfer & Reaction Engineering Lab, College of Chemical Engineering, Sichuan University, Chengdu, China 610065. Fax: 86 28 85460556; Tel: 86 28 85990133; Email: yuanshaojun@gmail.com*
[b] *Division of Materials Technology, School of Materials Science and Engineering, Nanyang Technological University, 50 Nanyang Avenue, 639798, Email: cleochoong@ntu.edu.sg*
[c] *Department of Environmental Sciences, University of Eastern Finland, 70211 Kuopio, Finland*

cellulose, gelatin, dextran, polyethylene and polystyrene.[27] Amongst them, Cytodex® dextran microcarriers are widely used in industrial scale cell cultivation.[28] However, they are not as suitable for use as cell delivery vehicles, as they can potentially manifest inflammatory responses, and this is evident in studies that have utilized Cytodex beads to potentiate inflammation and animal models.[29, 30] Hence, in order to develop a dual-functional microcarrier for both endothelial cell expansion and as injectable cell delivery vehicles, the material has to be ideally cytocompatible and cell adhesive, as well as biodegradable so that they do not persist at the tissue site.

Polycaprolactone (PCL), as one of biocompatible polyester with a degradation time of 2 – 4 years in vivo, has found multiple applications in tissue engineering.[31-34] While the rapid release of oligomers and acidic byproducts during the degradation of faster degrading polyesters, such as poly(L-lactide acid), could bring about the onset of acute inflammation,[35] PCL has demonstrated excellent long-term biocompatibility and minimal inflammatory responses in animal models.[36, 37] Furthermore, we and other researchers have modified PCL surfaces with cell-adhesive biomolecules such as gelatin and collagen via intermediate polymer brushes to improve its cytocompatibility.[38-40] Intermediate polymer brushes provide multiple reactive sites to conjugate increased amounts of biomolecules, and surface-initiated atom transfer radical polymerization (ATRP) is one strategy to grow polymer brushes on PCL surfaces.[39, 41-43]

Owing to the above mentioned biocompatibility and low immunogenicity, PCL is a suitable substrate material for endothelial-supporting microcarriers. In this study, PCL microspheres were synthesized by double emulsion solvent extraction/evaporation method and were further functionalized with novel poly(glycidyl methacrylate-azide) (PGMA-N_3) polymer brushes via surface-initiated ATRP. Azide-alkyne click chemistry between the azido groups on the PGMA-N_3 brushes and the alkynyl groups of hexynoic acid introduced the carboxylic functional groups (-COOH) on the PGMA-N_3 brushes, affording multiple reactive sites to covalently conjugate endothelial cell-adhesive REDV (Arg-Glu-Asp-Val) peptides via carbodiimide chemistry. Each intermediate functionalization step was ascertained using attenuated total reflectance Fourier transform infrared spectroscopy (ATR-FTIR), X-ray photoelectron spectroscopy (XPS) and scanning electron microscope (SEM). The REDV-immobilized PCL microspheres were then cultivated with human umbilical vein endothelial cells (HUVECs), and cell proliferation and viability assays were conducted in comparison with Cytodex® microcarrier beads as positive control.

2. Experimental

2.1 Materials

Polycaprolactone pellets (PCL, Mw 45000), poly(vinyl alcohol) (PVA, 87-89% hydrolyzed, Mw 85000), 1,6-hexanediamine (98%), 2-bromoisobutyrl bromide (BIBB, 98%), triethylamine (TEA, 98%), 2,2'-bipyridine (bpy, 99%), copper(I) bromide (CuBr, 99%), copper(II) bromide ($CuBr_2$, 98%), copper(II) sulfate ($CuSO_4$, 99%), sodium ascorbate (98%), sodium azide (NaN_3, 99%), ammonium chloride (NH_4Cl, 99.5%), 1-ethyl-3-(3-(dimethylamino)propyl) carbodiimide hydrochloride (EDC, 99%), 5-hexynoic acid (HA, 97%), and *N*-hydroxysuccinimide (NHS, 98%) were obtained from Sigma-Aldrich Chemical Co. (St. Louis, MO). The glycidyl methacrylate (GMA, 97%) monomer was obtained from Aladdin Inc. (Shanghai, China), and was passed through an inhibitor removal column prior to use. Solvents, such as isopropyl alcohol (IPA, 99.7%), hexane, toluene (anhydrous, 99%), methanol, ethanol, benzene, dimethyl sulfoxide (DMSO), *N,N*-dimethylformamide (DMF) and dichloromethane (anhydrous, >99.8%) were purchased from Kelong Reagent Co. (Chengdu, China). Arg-Glu-Asp-Val (REDV) short peptide was synthesized by ChinaPeptides Co. Ltd. (Shanghai, China), and was used without further purification. Human umbilical vein endothelial cells (HUVECs, ATCC CRL-1730) were obtained from the American Type Culture Collection (Manassas, VA). Cell culture medium (MCDB131), 4′,6′-diamidino-2-phenylindole (DAPI), heparin and paraformaldehyde (4%, w/v) were obtained from Sigma-Aldrich Chemical Co. Medium supplements, such as fetal bovine serum (FBS), Trypsin–EDTA (0.25%), bovine brain extract, amphotericin, penicillin, and streptomycin were purchased from Life Technologies (Carlsbad, CA). The MTT assay and the LIVE/DEAD cell viability kit were also obtained from Life Technologies. Cytodex®3 microcarrier beads (>175 μm) were purchased from Sigma-Aldrich Chemical Co.

2.2 Synthesis of azido-terminated GMA-N_3 monomer

The synthesis of GMA-N_3 monomer was achieved by the ring-opening reaction of epoxy groups using sodium azide (NaN_3). Typically, an aliquot of 9 mL (66 mmol) GMA monomer was introduced to a Pyrex® tube containing 100 mL of DMF. Subsequently, 4.272 g of NaN_3 (66 mmol) and 3.495 g (66 mmol) of NH_4Cl were added into the mixture solution. The transformation reaction was allowed to proceed at 50°C for 12 h under vigorous stirring. The addition of a protic or Lewis acid to the azide-epoxide mixture prevents the hydroxyl functional groups from participating in side reactions when the reaction is carried out in an aqueous solutions. After the reaction, rotary evaporation was used to reduce the solution volume to 15 mL. The concentrated solution was purified with column chromatograph and white liquid of GMA-N_3 was obtained. The structure of GMA-N_3 monomer was characterized by 1H-NMR (Bruker AV spectrometer, Bruker, Germany) and FTIR spectra (Perkin-Elmer Inc., Waltham, MA). 1H-NMR (600 MHz, $CDCl_3$, GMA-N_3) (ppm): 6.48 (2H), 6.40 (1H), 4.2-4.5 (4H), 3.8 (5H), 3.65 (6H), and 2.01 (3H) (ESI, Fig. S1b). The characteristic bands in the GMA-N_3 FTIR spectrum: 3500-3200 cm^{-1} (ν_{O-H}), 2115 cm^{-1} ($\nu_{N=N=N}$) and 1101 cm^{-1} (δ_{C-O}) (ESI, Fig. S2). The as-synthesized GMA-N_3 monomer was

subsequently used for surface functionalization of PCL microspheres.

2.3 Preparation of PCL microspheres and immobilization of ATRP initiator

PCL microspheres were prepared using a previously-established double emulsion solvent extraction/evaporation method (i.e. water-in-oil-in-water, W1/O/W2). Briefly, an aliquot of 2 g PCL pellets were dissolved into 20 mL dichloromethane to obtain 10% (w/v) oil (O) phase, while the dispersant PVA was dissolved into deionized water to obtain 0.2% (w/v) W1 phase. An aliquot of 2.5 mL of W1 solution was subsequently injected into the PCL solution and then sonicated for 30 s to form the W1/O emulsion. The W1/O emulsion was then injected into a 160 mL 0.5% (w/v) PVA aqueous solution (W2 phase) using syringe under continuous stirring. The resulting W1/O/W2 double emulsion was stirred continuously at 300 rpm for 2 h at room temperature for evaporating dichloromethane solvent. After the solidification, the PCL microspheres were harvested by centrifuge at a speed of 4000 rpm for 3 min, and washed with copious amount of deionized water thrice prior to being dried at room temperature in vacuum oven.

The surfaces of PCL microspheres were activated by aminolysis treatment in a 10% (w/w) isopropanol solution of 1,6-hexanediamine at 40^{o}C to introduce active amino groups using a previously-established procedure. The resultant aminolyzed PCL microspheres for 30 and 60 min were defined as the PCL-NH_2-1 and PCL-NH_2-2 surfaces, respectively. The immobilization of alkyl halide ATRP initiator was achieved by the TEA-catalyzed condensation reaction between the amino groups and 2-bromoisobutyrl bromide (BIBB). Briefly, the aminolyzed PCL microspheres were immersed in 20 ml of dried hexane solution containing 1.5 mL of triethylamine (TEA) and 0.5 mL of BIBB. The reaction was allowed to proceed at 0^{o}C for 2 h and then at room temperature for 24 h. After the reaction, the brominated PCL (defined as PCL-Br) microspheres were harvested with filtration and washed with copious amount of hexane and deionized water prior to being dried under reduced pressure. The PCL-Br microspheres from the PCL-NH_2-1 and PCL-NH_2-2 surfaces were referred to as the PCL-Br-1 and PCL-Br-2 surface, respectively.

2.4 Grafting of PGMA-N_3 brushes via surface-initiated ATRP

Surface-initiated ATRP reaction from the PCL-Br surfaces was carried out to graft PGMA-N_3 brushes using a [GMA-N_3]:[bpy]:[CuBr]:[$CuBr_2$] molar feed ratio of 50:2.0:1.0:0.2. Typically, an aliquot of 3 mL (about 17.0 mmol) of GMA-N_3 was introduced into a 25 mL round-bottom flask containing 5 mL of DMF. The reaction solution was purged with pure N_2 gas for 30 min to remove dissolved oxygen, followed by adding 24.3 mg (0.17 mmol) of CuBr, 7.58 mg (0.034 mmol) of $CuBr_2$ and 71 μL of bpy. The reaction tube was immediately sealed with rubber stopper to proceed ATRP reaction at 35^{o}C for 4 h. After the reaction, the resultant PGMA-N_3-grafted PCL microspheres (defined as PCL-*g*-PGMA-N_3) were filtered out and washed with copious amount of DMF, methanol and deionized water, in that order, to remove physically-adsorbed reactants prior to being dried under reduced pressure. The PGMA-N_3-grafted PCL microspheres from PCL-Br-1 and PCL-Br-2 surfaces were defined as PCL-*g*-PGMA1-N_3 and PCL-*g*-PGMA2-N_3 surfaces, respectively.

2.5 Carboxylation of PGMA-N_3 chains by azide-alkyne click reaction

The carboxylation of PGMA-N_3 brushes was accomplished by azide-alkyne click reaction between the pendant azido groups on the PGMA-N_3 side chains and the alkynyl groups of hexynoic acid. A 20 mg aliquots of PCL-*g*-PGMA-N_3 microspheres were immersed in a Pyrex® tube containing the mixture solution of DMSO (5 mL) and deionized water (5 mL), followed by adding 2 mL (18 mmol) of 5-hexynoic acid. The reaction solution was degassed with argon for 30 min under continuous stirring prior to the addition of 0.288 g (1.8 mmol) $CuSO_4$ and 0.732 g (3.6 mmol) of sodium ascorbate. The molar ratio of [HA]:[$CuSO_4$]:[$C_6H_7O_6Na$] was 10:1:2 for the azide-alkyne click reaction. The reaction tube was sealed immediately with the rubber stopper and kept in a 50^{o}C oil bath for 12 h to take place click reaction. At the end of the reaction, the carboxylated PCL microspheres (termed as the PCL-*g*-CPGMA-COOH) were washed with copious amount of ethanol and deionized water to move physically-adsorbed reactants, if any, prior to being dried under reduced pressure The carboxylated PGMA-N_3-grafted surfaces were denoted as the PCL-*g*-CPGMA1-COOH and PCL-*g*-CPGMA2-COOH surfaces, respectively.

2.6 Covalent immobilization of REDV peptides on the carboxylated PCL microsphere surfaces.

The click-coupled carboxyl groups (-COOH) on the CPGMA-COOH brushes were used as anchor sites to conjugate REDV short peptides via carbodiimide reaction. The PCL-*g*-CPGMA-COOH microspheres were pre-activated for 1 h at room temperature in a PBS solution (pH 7.4) containing 2 mg·mL^{-1} of NHS and 20 mg·mL^{-1} of EDC, and then the REDV peptides were added into the above PBS solution at a concentration of 5 mg·mL^{-1} under continuous stirring. The conjugation reaction mixture was allowed to proceed for 48 h at 25^{o}C to produce the PCL-*g*-CPGMA-*c*-REDV surfaces. After the reaction, the REDV-conjugated PCL microspheres were harvested by filtration and washed rigorously with copious amounts of PBS and deionized water to remove the physically-adsorbed REDV peptides prior to being dried under reduced pressure overnight.

2.7 Grafting density of PGMA-N_3 brushes and surface density of –COOH groups

The grafting density (GD) of PGMA-N_3 brushes and covalently-conjugated REDV peptides onto the PCL microsphere surfaces was evaluated by measuring weight change per surface area before and after grafting using a similar procedure described in detail previously.[44] The GD values were calculated according to the following equation:

$$GD = \frac{W_b - W_a}{A} \quad (1)$$

where W_a and W_b were the weights of the dry PCL microspheres before and after grafting of PGMA-N_3 brushes, respectively, and A was the surface area of PCL microspheres (about 0.64 cm^2). For the measurement of each GD values, at least three independent batches of PCL microspheres were investigated and the resulting values were averaged.

The surface density of –COOH groups on the carboxylated CPGMA-COOH chains was determined by a previously-established rhodamine-carboxyl interaction method.[45] Briefly, the PCL-*g*-CPGMA-COOH microspheres were dissolved in DMF solution to obtain polymer solution. The dye rhodamine 6G was dissolved in PBS solution (pH 12), and was immediately extracted with benzene to obtain benzene-dye reagent. An equal volume of polymer solution was mixed with benzene-dye for 10 min, and the absorbance of the solution at 530 nm was measured using a UV-VIS spectrophotometer (Pharmaspec UV-1700, Shimadzu). The absorbance of pristine PCL was measured as background control. A standard curve was established using known concentrations of 5-hexynoic acid dissolved in the benzene-dye solution. The concentration of carboxylic groups in the solution was calculated from the standard calibration curve.

2.8 Surface characterization.

The surface chemistry of the functionalized PCL microspheres was characterized by the measurement of ATR-FTIR and XPS spectra. The FTIR spectra were measured on a GX FTIR spectrometer (Perkin-Elmer Inc., Waltham, MA) equipped with a smart ATR performer accessory using a germanium (GE) with an incident angle of 45° and a sampling area of 2 mm^2 using a similar procedure described in detail previously.[39] The measurement of XPS spectra was performed on a Krato AXIS Ultra^{DLD} spectrometer with a monochromatic Al Kα X-ray source (1486.6 eV photons), using a previously reported procedure.[46] The change in surface morphology of the PCL microspheres at each functionalization step was characterized by SEM imaging. The functionalized PCL microspheres were sputter-coated with an ultrathin layer of platinum, and then mounted on a JSM 7500F SEM (JEOL, Tokyo, Japan) to capture SEM images at different magnifications. The mean size distribution and particle size of the PCL microspheres were determined by a wet laser scattering technique. The particle size measurements were performed at 25°C on a Winner2008 apparatus (Winner Particle Instrument Co., Jinan, China), equipped with a He-Ne laser operating at a wavelength of 632.8 nm and at a scattering angle of 90°. The CONTIN algorithm was used to analyze the obtained correlation functions. The average particle diameter (D_{av}) was the mean values from at least three batches of particles.

2.9 Cell proliferation and expansion assay on the functionalized PCL microspheres

Human Umbilical Vein Endothelial Cells (HUVECs) were used to assess the cytocompatibility of the PCL microspheres. The HUVEC culture procedures were described using a similar procedure described in detail previously.[38] HUVEC proliferation and viability on the microspheres was determined by MTT assay (3-(4,5-dimethyl)thiazol-2-yl-2,5-diphenyltetrazolium bromide). Prior to HUVEC seeding, the pristine PCL and functionalized PCL microspheres were sterilized with 70% ethanol for 2h, immersed in PBS solution (pH 7.4) for 2h, and then equilibrated in culture medium for 2h. An aliquot of 20 mg of microspheres was placed into a 24-well culture plate and 1 mL of a cell suspension (2×10^5 cell·mL^{-1} or 1×10^4 cells·mg^{-1}) was seeded into each cells for 1, 3, 5 and 7 days of incubation under a 5% CO_2 atmosphere at 37°C. Because the heavy adsorption of MTT agents by the PCL microspheres resulted in a significant deviation of cell numbers, the HUVECs cultured on the microsphere surfaces were detached by trypsinization using 0.5 mL of 0.25% Trypsin-EDTA solution at each predetermined incubation period. The detached HUVECs were incubated in 0.5 mL of fresh culture medium supplemented with 100 μL of MTT (5 mg·mL^{-1}), and then were continuously cultured for another 4 h. The MTT could be reduced to a formazan pigment by viable cells, which was dissolved by 0.5 mL of DMSO after the removal of the culture medium. The absorbance was measured at a wavelength of 560 nm for the working solution (200 μL) and 620 nm was used as a reference by a SpectraMax M2 Microplate Reader (Molecular Devices, Sunnyvale, CA, USA).

2.10 Cell viability and distribution on the functionalized PCL microspheres by fluorescence imaging

The fluorescent cell imaging by nuclear staining was used to assess HUVEC viability and expansion on the functionalized PCL microsphere surfaces. The functionalized PCL microspheres were incubated in a suspension of 2×10^5 cells·mL^{-1} at 37°C under a 5% CO_2 atmosphere. The culture medium was refreshed every other day. After 7 days of incubation, the PCL microsphere surfaces were washed with PBS solution and fixed with 4 wt% paraformaldehyde in PBS for 35 min at room temperature. 200 μL of 4′,6′-diamidino-2-phenylindole (DAPI) at 5 mg·mL^{-1} in PBS was added to each surface in a 24-well plate for 30 min at room temperature. The HUVEC-attached surfaces were washed twice with sterile PBS and mounted between glass slides with glycerol. DAPI-stained fluorescent images of HUVECs were captured under an excitation of 380 nm using a Nikon Image Ti Fluorescence microscope and the NIS-Elements Br software (Nikon Instruments Co., Tokyo, Japan). On the other hand, LIVE-DEAD stained fluorescence images were captured to evaluate cell coverage and viability. Similarly, the cell-microsphere constructs after 7 days of incubation were washed twice with sterile PBS solution, and then introduced the working solution containing 2 μM Calcein-AM and 4 μM EthD-1. After incubation at room temperature for 45 min, the microspheres were observed on the Nikon Image Ti Fluorescence microscope with

emission at 515 and 635 nm to acquire fluorescence images of the attached HUVECs.

2.11 Statistical analysis

All cellular experiments were performed with at least four replicates. Statistical analyses were carried out by one-way analysis of variance (ANOVA). A *p*-value of less than 0.05 was considered statistically significant. The quantitative results were expressed as mean ± standard deviation (SD).

3. Results and discussion

PCL microspheres tethered with the carboxylated CPGMA-REDV conjugates were achieved by the combination of surface-initiated ATRP and azide-alkyne click reaction, as schematically illustrated in Fig. 1. The synthesis process consisted of the following four steps: a) engrafting amino groups (-NH_2) onto the PCL microsphere surfaces by aminolysis treatment and subsequent introduction of alkyl bromide initiator by TEA-catalyzed condensation reaction between the amino groups on the PCL-NH_2 surfaces and 2-bromoisobutyryl bromide (BIBB), b) grafting of azido-terminated PGMA-N_3 brushes via surface-initiated ATRP of GMA-N_3, c) carboxylation of PGMA-N_3 brushes by azide-alkyne click reaction between the azido groups (N_3) on the PGMA-N_3 side chains and the alkynyl groups (C≡C) of hexynoic acid, and d) covalent conjugation of REDV short peptides to terminal carboxyl groups (-COOH) of the carboxylated CPGMA-COOH chains via carbodiimide chemistry to impart the biological cues for improved cell recognition. Success in each functionalization step was confirmed by the measurements of ATR-FTIR, XPS and SEM.

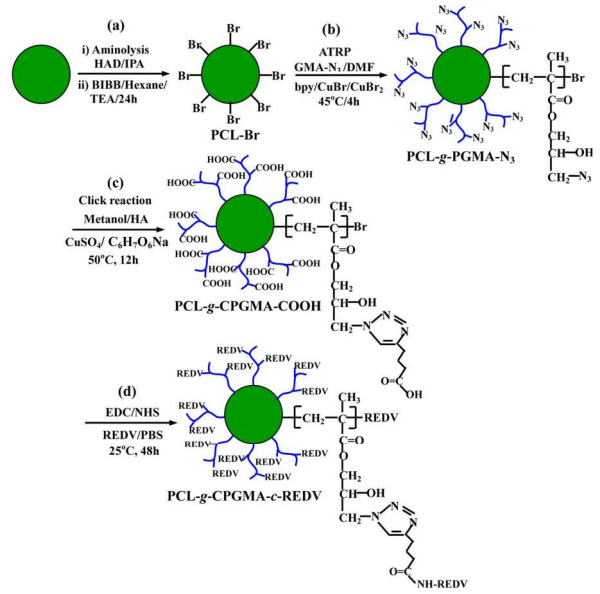

Fig. 1 Schematic illustration of the synthesis process of carboxylated CPGMA-REDV conjugates-grafted PCL surfaces: a) aminolysis treatment and immobilization of alkyl bromine initiator via TEA-catalyzed condensation reaction (the PCL-Br surface), b) grafting of azido-terminated PGMA-N_3 brushes via surface-initiated ATRP (the PCL-*g*-PGMA-N_3 surface), c) carboxylation of the PGMA-N_3 brushes by introducing hexynoic acid via azide-alkyne click reaction (the PCL-*g*-CPGMA-COOH surface), d) immobilization of REDV peptide onto the carboxylated CPGMA brushes via carbodiimide chemistry (the PCL-*g*-CPGMA-*c*-REDV surface).

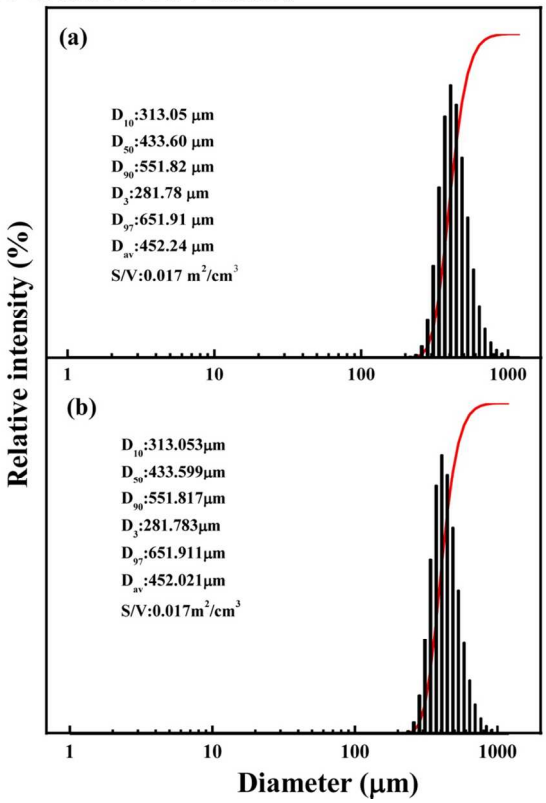

Fig. 2 Size distribution curves of the (a) pristine PCL and (b) PCL-Br-2 microspheres. The PCL microspheres were obtained from 10 wt% PCL solution at 300 rpm. The average diameters of the pristine PCL and brominated PCL-Br-2 microspheres were 452.24 and 452.02 μm, respectively.

3.1 Fabrication of PCL microspheres and Immobilization of ATRP initiator

PCL microspheres were fabricated by using a well-established double emulsion solvent extraction/evaporation method (i.e. water-in-oil-in-water, W1/O/W2). The particle size distribution of the as-synthesized PCL microspheres was characterized by the measurement of wet laser size analyzer. As shown in Fig. 2a, the PCL microspheres, which obtained with 10 wt% PCL solution at 300 rpm, had a relatively broad size distribution in a range of 250 - 900 μm, and their average diameter was about 452.24 μm (Table 1). It has been widely recognized that the initial concentration of oil phase (polymer solution) and stirring speed play a significant role in controlling particle size.[47, 48]

Due to its inherent inert nature (lack of active sites), the surfaces of PCL microspheres were aminolyzed to engraft reactive –NH_2 along the polyester chains.[49] Subsequently, TEA-catalyzed condensation reaction between the –NH_2 on the PCL-NH_2 surface and 2-bromoisobutyryl bromide (BIBB) took place to introduce an alkyl bromide-containing ATRP initiator. Fig. 3 showed the N 1s and Br 3d core-level XPS spectra of the PCL-NH_2

from 30 and 60 min of aminolysis reaction and PCL-Br microspheres, respectively. The appearance of a new N 1s

Table 1 The grafting density, surface compositions, and average diameters of the pristine PCL and functionalized PCL microspheres

Samples	GD[f] (mg·cm^{-2}) (mean ± SD)	[Br]/[C] [N]/[C][h]	CCG (μmol·cm^{-2})	Average diameter[i] (μm)
PCL	–	–	–	452.24
PCL-NH_2-1[a]	–	8.64×10^{-3}	–	451.76
PCL-NH_2-2[a]	–	2.14×10^{-2}	–	451.53
PCL-Br-1[b]	–	5.93×10^{-3}	–	452.16
PCL-Br-2[b]	–	1.43×10^{-2}	–	452.02
PCL-*g*-PGMA1-N_3[c]	0.326 ± 0.042	0.095	–	460.82
PCL-*g*-PGMA2-N_3[c]	1.078 ± 0.060	0.160	–	463.87
PCL-*g*-CPGMA1-COOH[d]	0.225±0.011	0.047	1.62±0.13	461.23
PCL-*g*-CPGMA2-COOH[d]	0.503±0.024	0.089	5.11±0.42	464.61
PCL-*g*-CPGMA1-*c*-REDV[e]	0.193±0.017	0.146	–	461.68
PCL-*g*-CPGMA2-*c*-REDV[e]	0.342±0.023	0.193	–	465.14

[a] PCL-NH_2-1 and PCL-NH_2-2 surfaces were obtained by immersing the PCL microspheres in a 10% (v : v) 1,6-hexanediamine/2-propanol solution for 30 and 60 min at 40°C, respectively. [b] PCL-Br-1 and PCL-Br-2 surfaces were obtained from the PCL–NH_2-1 and PCL–NH_2-2 surfaces, respectively, after 24 h of reaction with 2-bromoisobutyryl bromide (BIBB) in dried hexane containing 1 : 1 (molar ratio) BIBB and triethylamine (TEA). [c] Reaction conditions: [GMA-N_3]:[CuBr]:[$CuBr_2$]:[bpy] = 50:1:0.2:2 in a mixture aqueous solution of methanol and deionized water (v:v, 5:1) at 35°C for 4h. [d] Reaction conditions: [HA]:[$CuSO_4$]:[$C_6H_7O_6Na$] = 10:1:2 in a mixture solution of methanol and deionized water (v:v, 5:1) at 50°C for 12h. [e] Reaction conditions: the PCL-*g*-CPGMA-COOH surfaces were incubated in a PBS buffer (pH 7.4) containing 10:1 (molar ratio) EDC and NHS at 25°C for 1 h, and were subsequently transferred into a PBS solution containing REDV peptide at a concentration of 5 mg/ml at 25°C for 48 h. [f] Grafting density (GD) is defined as GD = (W_b – W_a)/A, where W_a and W_b correspond to the weight of the dry microspheres before and after grafting of polymer brushes, respectively, and A is the surface area of microsphere. SD denotes standard deviation. [g] CCG represents the surface density of carboxyl groups (-COOH) on the CPGMA-COOH brushes determined by the rhodamine-carboxyl interaction method. [h] The elemental ratio was determined from the sensitivity factor-corrected C 1s, N 1s and Br 3d core-level spectral area ratios. [i] The average diameters of PCL microspheres were determined by the wet laser size analyzer measurement.

signal with binding energy (BE) at 400 eV after aminolysis (ESI, Figs. S3c and S3e) and subsequent appearance of three additional signals at 70 (Br 3d), 189 (Br 3p) and 256 eV (Br 3s) in the wide scan XPS spectra (ESI, Figs. S4a and S4c) were indicative of successful engraftment of –NH_2 and immobilization of alkyl bromide-containing ATRP initiator, respectively. The [N]/[C] ratios, as determined from sensitivity factor corrected N 1s and C 1s core-level XPS spectral areas, were 8.64×10^{-3} and 2.14×10^{-2} for the PCL-NH_2-1 (Fig. 3a) and PCL-NH_2-2 (Fig. 3b) microsphere surfaces, respectively. This result was consistent with the previous findings that prolonging aminolysis reaction time resulted in the increase in surface density of –NH_2 on the PCL substrates.[50] Correspondingly, the surface ratios of [Br]/[C] increased from 5.93×10^{-3} for the PCL-Br-1 (Fig. 3c) to 1.43×10^{-2} for the PCL-Br-2 surfaces (Fig. 3d), suggesting that higher surface density of –NH_2 led to the increase in surface density of ATRP initiator. Upon the aminolysis treatment, the PCL microsphere underwent a slight decrease in particle size to 451.53 μm after 60 min of reaction (Table 1), since the aminolysis reaction took place preferentially at the amorphous regions of polymer and hence resulted in the bulk degradation in diamine solution.[49] The average particle diameter of PCL-Br-2 microspheres increased slightly to 452.02 μm (Fig. 2b). Thus, the alkyl bromide-containing ATRP initiators were ascertained to be immobilized on the aminolyzed PCL microspheres to cater for further functionalization.

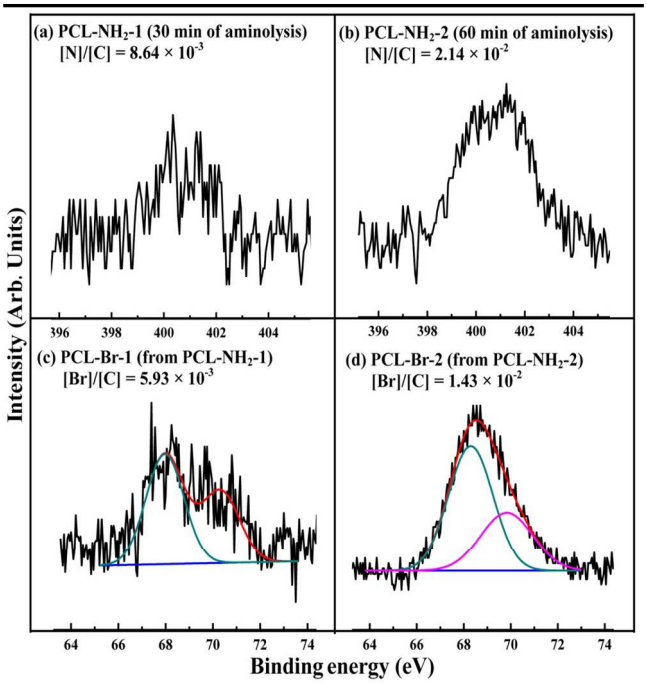

Fig. 3 N 1s and Br 3d core-level spectra of the (a) PCL-NH_2-1 (from 30 min of aminolysis), (b) PCL-NH_2-2 (from 60 min of aminolysis), (c) PCL-Br-1 (from PCL-NH_2-1 surface),and (d)

PCL-Br-2 surfaces (from PCL-NH_2-2 surface). The appearance of additional Br signals indicated successful immobilization of alkyl bromide-containing ATRP initiator on the aminolyzed PCL microsphere surfaces.

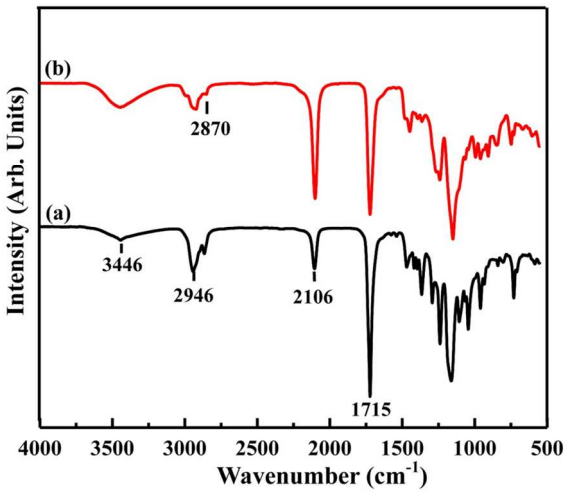

Fig. 4 ATR-FTIR spectra of the (a) PCL-*g*-PGMA1-N_3 (from the PCL-Br-1 surface) and (b) PCL-*g*-PGMA2-N_3 (from the PCL-Br-2 surface) microspheres after 4 h of ATRP reaction. Successful grafting of PGMA-N_3 brushes can be deduced from the appearance of characteristic azide band with wavenumber at 2106 cm^{-1}.

3.2 Grafting of azido-terminated PGMA-N_3 brushes via surface-initiated ATRP

The azido-terminated GMA-N_3 monomer was synthesized by the ring-open reaction of the oxirane groups of GMA and sodium azide, and characterized by 1H-NMR and FTIR (ESI, Figs. S1 and S2). The surface-initiated polymerization took place from the PCL-Br surfaces for 4 h with the molar ratio of [GMA-N_3 (monomer)]:[CuCl (catalyst)]:[$CuCl_2$ (deactivator)]:[byp (ligand)] at 50:1:0.2:2 to produce the PCL-*g*-PGMA-N_3 microsphere surfaces. Fig. 4 showed the FTIR spectra of the PCL-*g*-PGMA1-N_3 (from the PCL-Br-1 surface) and PCL-*g*-PGMA2-N_3 (from the PCL-Br-2 surface), respectively. Successful grafting of PGMA-N_3 brushes on the microsphere surfaces was affirmed by the characteristic bands with a wavenumber at 2106 cm^{-1}, attributable to the stretching vibration of azido groups ($\nu_{N^+=N=N^-}$).[51] The relatively stronger intensity of azido groups on the PCL-*g*-PGMA2-N_3 surface (Fig. 4b) than that of the PCL-*g*-PGMA1-N_3 surface (Fig. 4a) suggested a higher surface density of azido groups on the PCL-*g*-PGMA2-N_3 surface. Another additional band at the wavenumber at 3446 cm^{-1} (the stretching vibration of O-H ν_{O-H}), characteristic of the hydroxyl groups of PGMA-N_3 side chains, also confirmed the success in grafting of PGMA-N_3 brushes on the PCL microsphere.

The chemical composition of azido-terminated PGMA-N_3-grafted microsphere surfaces was also ascertained by XPS characterization. Fig. 5 showed the respective wide scan, C 1s and N 1s core-level spectra of the PCL-*g*-PGMA1-N_3 and PCL-*g*-PGMA2-N_3 surface. The appearance of an additional N 1s signal (with BE at about 400 eV) in the wide scan XPS spectra indicated the successful grafting of PGMA-N_3 brushes on the PCL

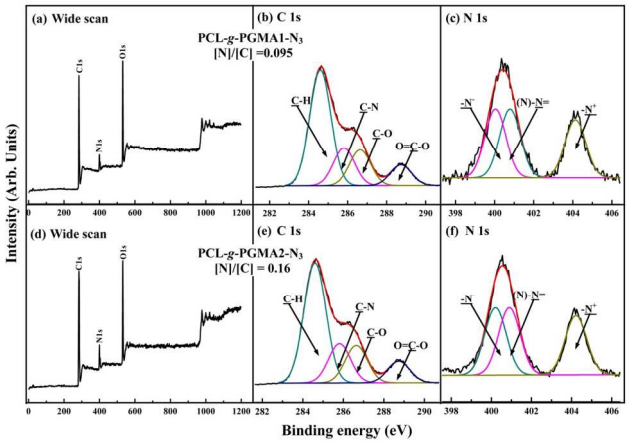

Fig. 5 Wide scan, C 1s and N 1s core-level XPS spectra of (a-c) PCL-*g*-PGMA1-N_3 (from the PCL-Br-1 surface) and (d-f) PCL-*g*-PGMA2-N_3 microsphere surfaces (from the PCL-Br-2 surface) microspheres after 4 h of ATRP reaction. The additional N 1s signal in the wide scan spectra, the C-N characteristic peak in the C 1s core-level spectra, as well as the characteristic $–N^+$, -N= and $–N^-$ peak components in the N 1s core-level spectra were consistent with successful grafting of PGMA-N_3 brushes on the PCL microsphere surfaces, as compared to those of the PCL-Br surfaces.

microsphere surfaces (Figs. 5a and 5d). The curve-fitted C 1s core-level spectra consisted of four peak components with BEs at 284.6, 285.5, 286.2 and 288.8 eV, attributable to C-H, C-N, C-O and O=C-O species[52] (Figs. 5b and 5e), respectively. The novel characteristic C-N species was associated with the pendant azido groups in the PGMA-N3 chains. The N 1s core-level spectra was curve-fitted with three peak components with BEs at 399.9, 401.2 and 404.6 eV, attributable to the negatively charged nitrogen ($-N^-$), the imine nitrogen (-N=), and the positively charged nitrogen ($-N^+$),[52] respectively (Figs. 5c and 5f). The molar ratio of the three peak components was close to 1:1:1, as determined from the spectral area ratio of the three species. This result was consistent with the theoretical ratio of the chemical structure of azido groups ($-N=N^+=N^-$). On the other hand, the [N]/[C] ratios for the PCL-*g*-PGMA1-N_3 and PCL-*g*-PGMA2-N_3 surfaces were determined to be 0.095 and 0.16, respectively, indicative of higher surface density of the azido groups on the PCL-*g*-PGMA2-N_3 surfaces. The increase in the average particle diameter to 460.82 μm for the PCL-*g*-PGMA1-N_3 and 463.87 μm for the PCL-*g*-PGMA2-N_3 microspheres further confirmed the presence of polymer brushes on the PCL microsphere surfaces (Table 1, ESI, Figs. S5a and S5b). Thus, the azido-terminated PGMA-N_3 brushes were successfully grafted onto the PCL microsphere surfaces and their

surface density was dependent on the surface concentration of the ATRP initiator.

The grafting density (GD) of the PGMA-N_3 chains was measured to determine their growth kinetics on the PCL microspheres (ESI, Fig. S6). An approximate linear in increase in the GD values of the PGMA-N_3 brushes with reaction time suggested that the chain growth occurred in a time-dependent manner. On the other hand, the GD values of the PGMA-N_3 brushes were around 0.326 ± 0.042 and 1.076 ± 0.060 mg·cm^{-2} for the PCL-*g*-PGMA1-N_3 and PCL-*g*-PGMA2-N_3 surfaces after 4 h of reaction, respectively (Table 1), which affirmed the increase in GD of polymer brush with the surface density of initiator sites. These results are consistent with the previous findings that the surface density of initiator sites plays a crucial role in determining the number of growing polymer chains and the grafting density of polymer brushes.[53, 54]

3.3 Carboxylation of PGMA-N_3 brushes by azide-alkyne click reaction

The pendent azido groups in the PGMA-N_3 chains offered an attractive platform to initiate the Cu(I)-catalyzed Huisgen 1,3-dipolar cycloaddition reaction for the introduction of complex functional moieties and/or biomolecules.[55] In this study, the carboxylation of PGMA-N_3 brushes was achieved by Cu(I)-catalyzed azide-alkyne click reaction to provide reactive carboxyl groups (-COOH). ATR-FTIR spectra of the carboxylated polymer brush, termed PCL-*g*-CPGMA-COOH surfaces, showed the disappearance of the characteristic –N≡N band with a wavenumber at 2106 cm^{-1}, the appearance of a broad band at about 3600-3200 cm^{-1}, attributable to H-bonded O-H stretching vibration (ν_{O-H}), as well as an additional moderate peak at 1565 cm^{-1}, attributable to the N=N stretching vibration ($\nu_{N=N}$)[56] (ESI, Fig. S7). Successful carboxylation of the PGMA-N_3 brushes was also ascertained by XPS characterization, and the XPS spectra of the PCL-*g*-CPGMA-COOH surfaces were shown in Fig. 6. The decrease in the relative intensity of N 1s signal (BE at around 400 eV) (Figs. 6a and 6d), as well as the decreased in the [N]/[C] ratio to around 0.047 for the PCL-*g*-CPGMA1-COOH and 0.089 for the PCL-*g*-CPGMA2-COOH surfaces (Table 1), indicated the successful coupling of hexynoic acid onto the PGMA-N_3 brushes. The introduction of COOH groups was further verified by evident increase in the relative amount of characteristic O=C-O peak component in the curve-fitted C 1s core-level XPS spectra (Figs. 6b and 6e). Another distinct feature was observed on the curve-fitted N 1s core-level spectra for the PCL-*g*-CPGMA-COOH surfaces, which consisted of two peak components with BEs at 399.7 and 401.8 eV, attributable to the imine (=N-) and amine (–N-) species,[57] respectively (Figs. 6c and 6f). The [=N-]/[-N-] area ratio of 2:1 was consistent with the formation of a triazole moiety in the azide-alkyne click reaction process.[57] According to the well-established colorimetric method, the surface densities of the –COOH groups on the PCL-*g*-CPGMA1-COOH and PCL-*g*-CPGMA2-COOH surfaces were determined to be 1.62 ± 0.13 and 5.11 ± 0.42 μmol·cm^2, respectively (Table 1). With the click coupling of hexynoic acid, the average particle diameters slightly increased to 461.23 μm for the PCL-*g*-CPGMA1-COOH and 464.61 μm for the PCL-*g*-CPGMA2-COOH microspheres (Table 1, ESI, Fig. S5c).

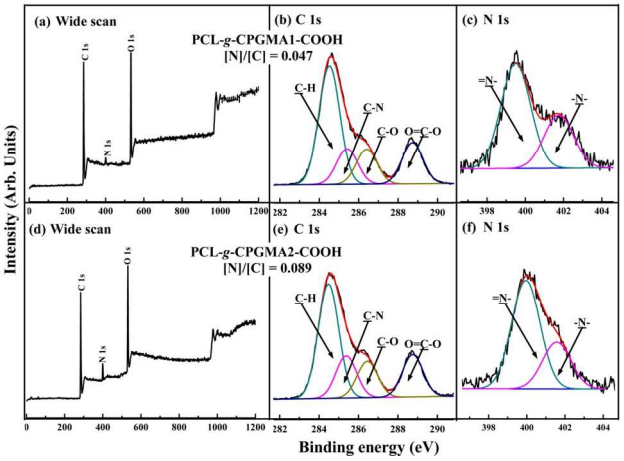

Fig. 6 Wide scan, C 1s and N 1s core-level XPS spectra of the (a-c) carboxylated PCL-*g*-CPGMA1-COOH and (d-f) PCL-*g*-CPGMA2-COOH microsphere surfaces after the introduction of hexynoic acid via azide-alkyne click reaction. Successful carboxylation of PGMA-N_3 brushes was ascertained by the increase in relative amount of O=C-O$^-$ species in the C 1s core-level spectra and the characteristic –N- and –N= peak components in the N 1s core-level spectra.

3.4 Covalent immobilization of REDV peptides onto the carboxylated PCL microsphere surfaces

Arg-Glu-Asp-Val (REDV) short peptide, as a primary amino acid sequence derived from fibronectin, was one of the main recognition sites for integrin $\alpha_4\beta_1$ receptors on the endothelial cell surface, which led to specific interactions between fibronectin and endothelial cells.[58] Integrin-mediated binding of cells has been found to be the foundation for cell growth and differentiation and to be the dominant mechanism by which cells communicate with noncellular surroundings.[59] Hence, REDV peptide has been widely incorporated into biomaterial matrix to trigger the selective and specific interaction between endothelial cells and substrates.[60-62] In this work, the abundant –COOH groups on the side chains of CPGMA-COOH brushes provided versatile anchor sites for the immobilization of biologically-active molecules. To covalently conjugate the REDV peptides onto the carboxylated PCL microspheres, the –COOH groups on the CPGMA-COOH chains were pre-activated by the EDC/NHS chemistry to introduce reactive esters (succiniimidyl intermediates).[63] The nucleophilic substitution reaction between the active esters and the amine groups of REDV peptides eventually resulted in a stable amide linkage (O=CNH) between REDV and the CPGMA-COOH brushes.

Fig. 7 showed the FTIR spectra of the pure REDV, PCL-*g*-CPGMA1-*c*-REDV and PCL-*g*-CPGMA2-*c*-REDV microsphere surfaces. The main characteristic bands of REDV peptides included a broad band of overlapping O-

H/N-H stretching vibration with wavenumber at 3250–3600 cm^{-1} (ν_{O-H} at about 3400 cm^{-1} and ν_{N-H} at about 3250 cm^{-1}), amide I ($\nu_{C=ONH}$) at 1635 cm^{-1} and amide II (δ_{N-H}) at 1550 cm^{-1} (Fig. 7c), respectively. Successful immobilization of REDV peptides on the azido-terminated

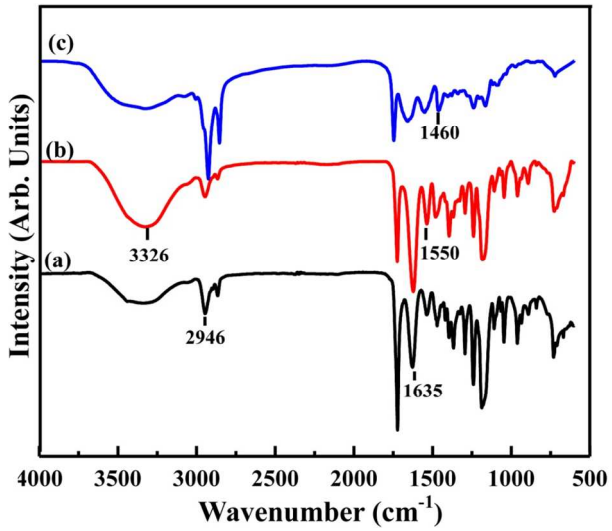

Fig. 7 ATR-FTIR spectra of the (a) PCL-*g*-CPGMA1-*c*-REDV, (b) PCL-*g*-CPGMA2-*c*-REDV microsphere surfaces, and (c) pure REDV peptide. The presence of a broad band of free O-H and N-H (at 3326 cm^{-1}), amide I band (at 1635 cm^{-1}) and amide II (at 1550 cm^{-1}) as compared to that of the pure REDV peptides.

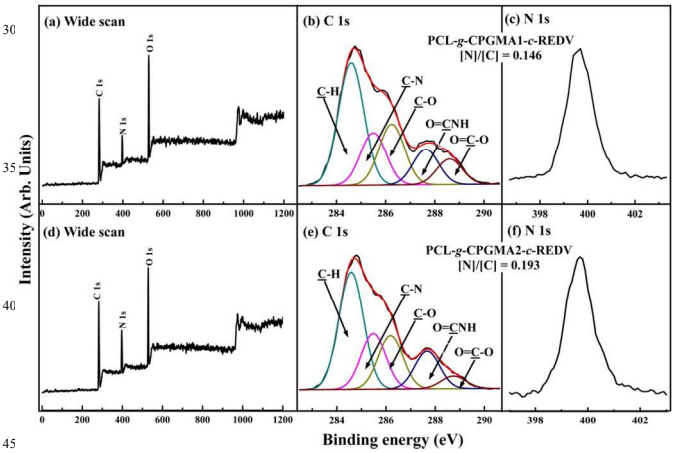

Fig. 8 Wide scan, C 1s and N 1s core-level XPS spectra of the (a-c) PCL-*g*-CPGMA1-*c*-REDV and (d-f) PCL-*g*-CPGMA2-*c*-REDV microsphere surfaces. The appearance of additional O=CNH peak component in the C 1s core-level spectra as a result of immobilized REDV peptides.

CPGMA-COOH brushes could be deduced from the appearance of three additional bands at 3250-3600 cm^{-1} for $\nu_{O-H/N-H}$, 1635 cm^{-1} for $\nu_{C=ONH}$ and 1550 cm^{-1} for δ_{N-H}, as well as the disappearance of the characteristic band at 2106 cm^{-1} for the stretching vibration of azido groups (Figs. 7a and 7b). Furthermore, the relative intensity of these three new bands for the PCL-*g*-CPGMA2-*c*-REDV surfaces was evidently stronger than those for the PCL-*g*-CPGMA1-*c*-REDV surface, indicative of the high surface density of the immobilized REDV peptides on the former microsphere surface.

The REDV-immobilized PCL surfaces were also characterized by XPS, and the results were shown in Fig. 8. The significant increase in the relative intensity of N 1s signal in the wide scan XPS spectra was indicative of the presence of REDV peptides on the microsphere surfaces (Figs. 8a and 8d). The curve-fitted C 1s core-level spectra for the REDV-immobilized surfaces consisted of five peak components with BEs at 284.6, 285.5, 286.2, 287.8 and 288.6 eV, attributable to the C-H, C-N, C-O, O=C-NH and O=C-O species,[52] respectively (Figs. 8b and 8e). The characteristic O=C-NH species was associated with the linkages in REDV peptide itself, as well as the linkage between the CPGMA-COOH brushes and REDV peptide.[64] The only neutral amino groups with BE at 399.8 eV in the curve-fitted N 1s core-level spectra was consistent with the successful immobilization of REDV peptide onto the carboxylated PCL-*g*-CPGMA-COOH surfaces (Figs. 8c and 8f). The [N]/[C] ratios, as determined from the N 1s and C 1s core-level spectral area ratio, were about 0.146 for the PCL-*g*-CPGMA1-*c*-REDV and 0.193 for PCL-*g*-CPGMA2-*c*-REDV surfaces (Table 1), which was further evidence of higher amount of the REDV peptides immobilized on the PCL-*g*-CPGMA2-COOH surfaces. This result was consistent with the fact that the grafting density of REDV peptides was dependent on the surface density of the –COOH groups on the CPGMA-COOH brushes. This point was further affirmed by the higher grafting density of REDV peptides for the PCL-*g*-CPGMA2-*c*-REDV at about 0.342 ± 0.023 $mg \cdot cm^{-2}$ than that for PCL-*g*-CPGMA1-*c*-REDV at 0.193 ± 0.017 $mg \cdot cm^{-2}$ (Table 1). The conjugation of REDV peptides onto the carboxylated CPGMA-COOH-grafted surfaces further resulted in a slight increase of the average particle size to about 461.68 μm for the PCL-*g*-CPGMA1-*c*-REDV and about 465.14 μm for the PCL-*g*-CPGMA1-*c*-REDV microsphere surfaces (Table 1, ESI, Fig. S5d). Thus, the above results were consistent with the successful immobilization of REDV peptide on the PCL microsphere surface, and the surface density of REDV peptides was positively correlated with the surface grafting density of –COOH groups on the CPGMA-COOH brushes.

3.5 Surface Morphology

The change in surface morphology of the PCL microspheres after each modification step was characterized by SEM imaging, and the representative SEM images of the pristine PCL and functionalized PCL microspheres were shown in Fig. 9. The pristine PCL microsphere showed a smooth surface with a broad size distribution (Figs. 9a1-9a3), which was consistent with the particle size distribution results from laser scattering characterization. Aminolysis treatment and subsequent bromination reaction of the PCL microspheres resulted in a slight increase in surface roughness (Figs. 9b1-9b3), and shallow micropits were also observed on the PCL-Br-2 surfaces, which was mainly ascribed to the degradation nature of the aminolysis reaction (Fig. 9b3). Previous

studies have reported that hexamediamine molecules could penetrate into the amorphous region of polymer matrix, and the aminolysis reaction took place at a depth of around 50 μm.[65] Upon grafting of PGMA-N_3 brushes, the microsphere surfaces not only showed a fairly rougher

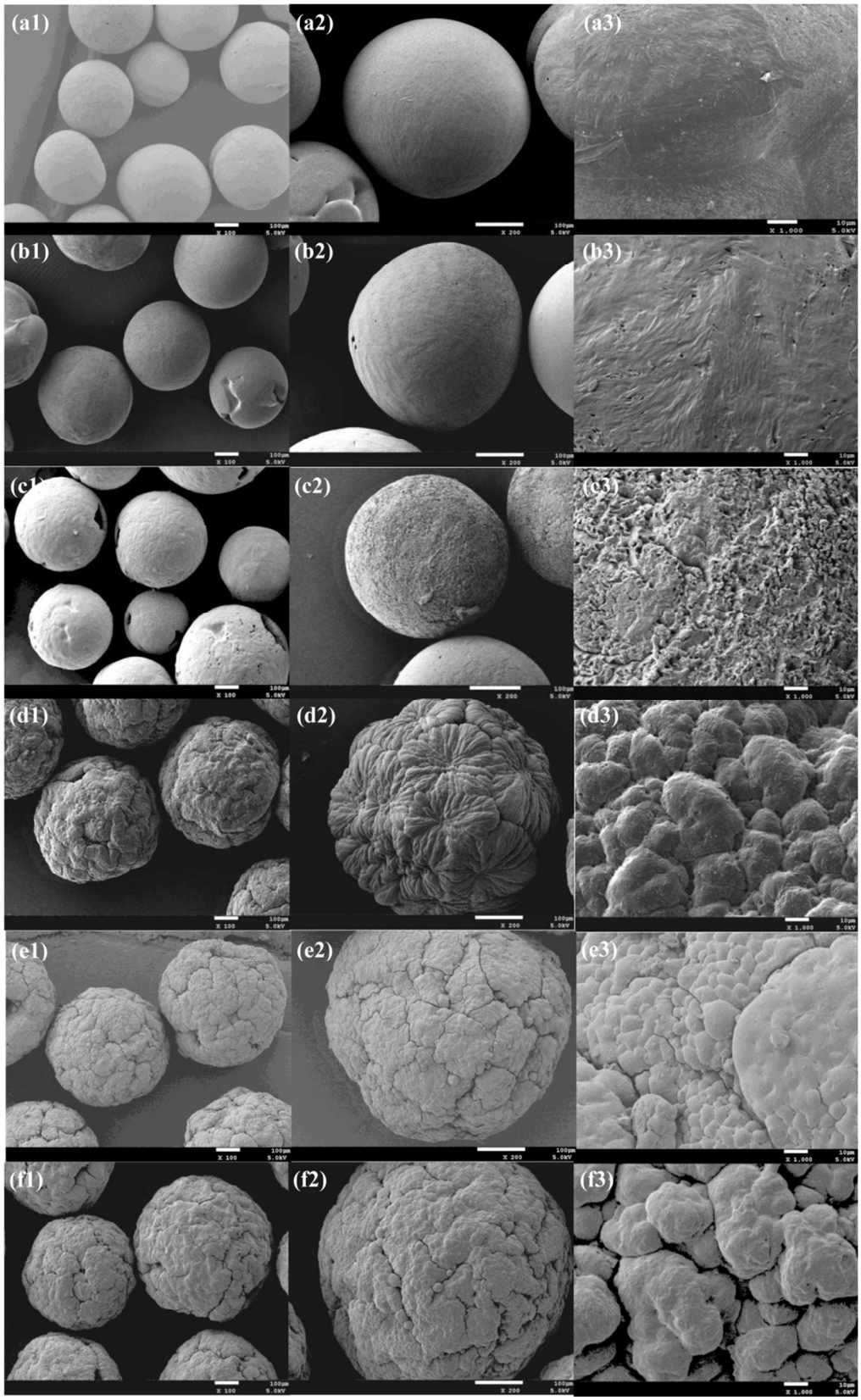

Fig. 9 SEM images at different magnification (100×, 200×, 1000×) for the surface morphology of the (a1-a3) pristine PCL, (b1-b3) PCL-Br-2, (c1-c3) PCL-*g*-PGMA1-N_3, (d1-d3) PCL-*g*-PGMA2-N_3, (e1-e3) PCL-*g*-CPGMA2-COOH, and (f1-f3) PCL-*g*-CPGMA2-REDV microspheres

surface as compared to the pristine PCL and brominated PCL microsphere surfaces, but also gave rise to a porous microstructure (Figs. 9c1-9d3). Especially for the PCL-*g*-PGMA2-N_3 microsphere surface (Figs. 9d1-9d3), dense and thick polymer coatings with fibre-like features were evidently observed, indicating that higher surface density of initiators could result in a complete and thick coverage of PGMA-N_3 brushes. This result was well consistent well with the increase in the average particle diameter obtained from laser scattering measurements. Subsequent coupling of hexynioc acid via azide-alkyne click reaction appeared to proceed in a relatively uniform manner, as the PCL-*g*-CPGMA2-COOH surface showed a thicker polymeric coating but decrease in microstructure roughness (Figs. 9e1-9e3). The covalent conjugation of REDV peptides further caused a slight increase in porous microstructure and roughness of the PCL-*g*-CPGMA2-*c*-REDV microsphere surfaces (Figs. 9f1-9f2). Taken together, the grafting of CPGMA-REDV conjugates virtually led to the evident increase in surface roughness and porous microstructure.

3.6 Endothelial cell proliferation and expansion on the functionalized PCL microspheres

In this work, the HUVECs cultured on the PCL microsphere surfaces were detached by trypsinization before the MTT assay in order to eliminate the interference of the adsorption of MTT agents by the microsphere scaffolds. Thus, the HUVECs proliferation on the REDV-immobilized PCL microspheres, together with the Cytodex® microcarrier beads served as positive controls, was kinetically monitored and quantitatively evaluated by the MTT assay over the course of 7 days. By correlating MTT assay readings of cells to actual viable cell numbers, the number of cells at the end of each alternate day could be determined on each type of PCL microsphere surface.

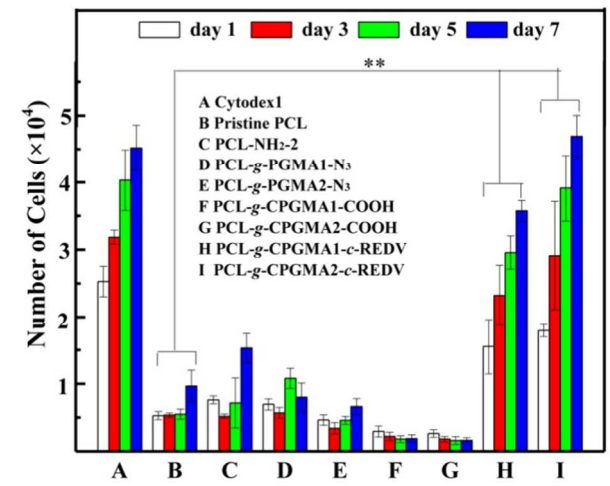

Fig. 10 Proliferation of HUVECs on the different surfaces of PCL microspheres as assessed by the MTT assay. Data is denoted as mean ± SD. *p<0.05 and **p<0.01 refer to the statistically significant difference with respect to the pristine PCL microspheres. The cell proliferation rate of HUVECs seeded on the REDV-immobilized surfaces was significantly improved as compared to that the pristine PCL microsphere.

Fig. 10 showed the proliferation profiles of the attached HUVECs on the pristine PCL and functionalized PCL microspheres as a function of culture time. HUVEC proliferation over the course of 7 days was largely determined by initial attachment (at the end of day 1) and cumulative population doublings over a period of 7 days. Poor support for the HUVEC growth was evident on the pristine PCL microspheres, which was in good agreement with the previous studies that the intrinsic hydrophobic nature and the lack of cell-recognition motifs of PCL were unfavorable for cellular attachment and growth. [66, 67] Initial HUVEC attachment (at end of day 1) was poor on the pristine PCL, PGMA-N_3-grafted PCL and carboxylaed CPGMA-COOH-grafted PCL microsphere surfaces, which accounted for poor growth by day 7. Grafting of PGMA-N_3 and carboxylated CPGMA-COOH brushes did not lead to the improvement HUVEC attachment and proliferation, in spite of the observed increase in surface roughness and porous microstructures and improved surface hydrophilicity (-OH groups present on the former surface, whilst –COOH groups on the latter surfaces). It has been widely accepted that polymer surfaces with moderate hydrophilicity of water contact angles in a range of 40–70^o and rougher miro/nanotopography are favorable for cell adherence and proliferation.[68] Particularly, the –COOH groups present on the carboxylated CPGMA-COOH-grafted PCL surfaces appeared to have a detrimental effect on cell attachment and growth, as the cell number decreased with increasing incubation time and increase in surface density of –COOH groups. As a matter of fact, this results was well consistent with previous findings that anionically-charged –COOH groups were resistant to cell attachment due to electrostatic repulsion.[69]

A slight improvement in initial HUVEC adhesion and growth was observed on the aminolyzed PCL-NH_2-2 microsphere surfaces as compared to the pristine PCL and PGMA-N_3-grafted surfaces, which was in agreement with previous studies that the presence of amino groups (-NH_2) improved surface hydrophilicity and initial cell adhesion.[69] However, once REDV peptide was conjugated onto the side chains of CPGMA-COOH brushes, termed as PCL-*g*-CPGMA-*c*-REDV surfaces, initial HUVEC attachment and proliferation were found to be significantly enhanced in comparison with other modified PCL microspheres as a result of the positive cell-material interactions from the presence of the bioactive REDV peptide motifs. In fact, cell numbers on PCL-*g*-CPGMA2-*c*-REDV microspheres over the course of 7 days were comparable to those on the positive control of Cytodex® microcarrier beads. The HUVEC growth appeared to be in a manner dependent on the surface density of the immobilized REDV peptides, as

the PCL-*g*-CPGMA2-*c*-REDV surface yielded better HUVEC adhesion and population doublings than the PCL-*g*-CPGMA1-*c*-REDV surface, thus leading to the best surface for supporting HUVEC growth. Theoretically, each –COOH groups can covalently affix an individual REDV peptide molecule, the immobilized collagen on the side chains of CPGMA-COOH brushes would be in a dispersed manner rather than in a continuous surface layer. As a result, the higher surface density of REDV peptides, the better for the proliferation and expansion of HUVECs. Taken together, the PCL-*g*-CPGMA-*c*-REDV microsphere surfaces with a higher surface density of REDV peptides, together with rougher micro/nano-structured topography and moderate hydrophilicity, provided abundant epitopes or ligands for cell anchoring and proliferation, thus making the PCL microspheres highly conducive for endothelial cell expansion.

3.7 Cell coverage and viability of HUVECs on the functionalized PCL Microspheres

The HUVEC coverage and viability on the functionalized PCL microsphere surfaces on day 7 visualized by nuclear DAPI and LIVE/DEAD® staining provided a good assessment of the extent of cell expansion, and the representative fluorescent images were as shown in Fig. 11. The pristine PCL microsphere surface exhibited lower cell coverage, as HUVECs were sparsely distributed over the microsphere surfaces (Figs. 11a and 11b). This result further affirmed the poor cell affinity and growth on the pristine PCL microspheres. The even lower HUVEC coverage on the PCL-*g*-CPGMA2-COOH microsphere surfaces (Figs. 11c and 11d) further verified the inhibitive feature of the –COOH groups for cell attachment and growth. In contrast, the incorporation of cellular motifs onto the PCL microspheres surfaces resulted in dense coverage of HUVECs regardless of surface density of the immobilized REDV peptides, and a confluent layer of HUVECs was evidently covered on the PCL-*g*-CPGMA1-*c*-REDV (Figs. 11e and 11f) and PCL-*g*-CPGMA2-*c*-REDV(Figs. 11g and 11h) surfaces after 7 days of culture. This result was further evidence that the cell proliferation of HUVECs on the REDV-immobilized PCL microsphere surfaces were substantially improved for cell expansion, which was in good agreement with the cell proliferation data. The confluency extent of HUVECs covered on the microsphere surfaces was found to be positively correlated with the surface density of the immobilized REDV peptide, as the HUVECs were distributed more densely on the periphery of the PCL-*g*-CPGMA2-*c*-REDV microspheres. In addition, calcein-AM (green fluorescence) stains for viable cells in the LIVE/DEAD® viability staining. The observation that the HUVECs were stained green, and were thus viable on the PCL-*g*-CPGMA1-*c*-REDV and PCL-*g*-CPGMA2-*c*-REDV microspheres (Figs. 11f and 11h), which also complemented the MTT assay conducted to measure viable cell numbers on day 7. In short, the optimally-functionalized PCL-*g*-CPGMA2-*c*-REDV microsphere surfaces, which was derived from the combination process of surface-initiated ATRP and click reaction, was able to trigger rapid cell attachment, proliferation and expansion, hence it was potentially useful for the vascular implants.

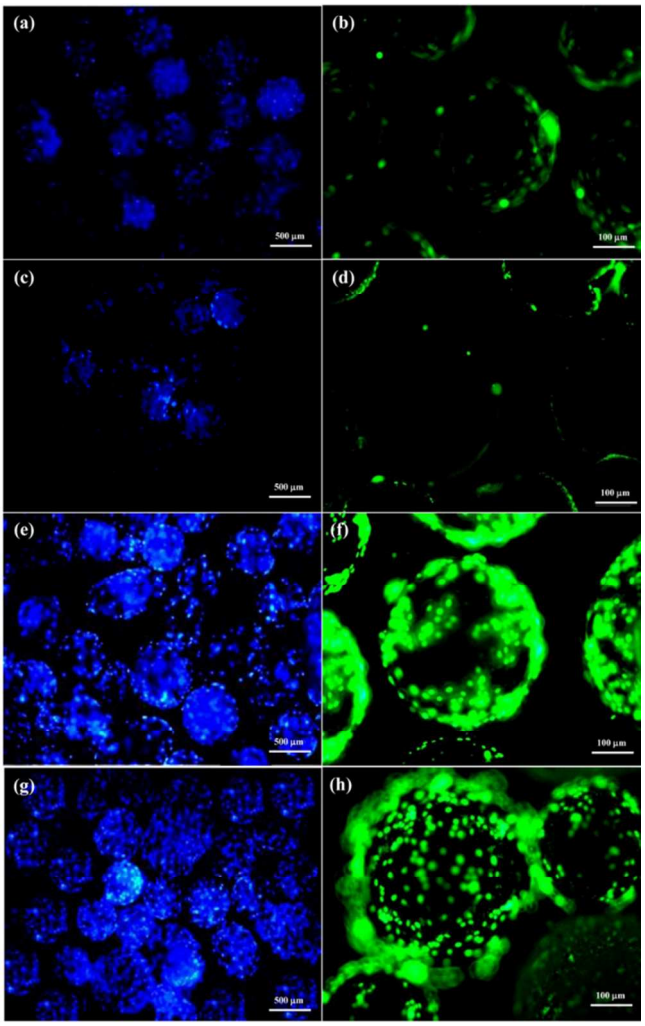

Fig. 11 Representative fluorescence images of (a,c,e,g) DAPI staining and (b,d,f,h) LIVE/DEAD® staining of HUVECs cultured on the surfaces of pristine PCL, PCL-*g*-CPGMA2-COOH, PCL-*g*-CPGMA1-*c*-REDV and PCL-*g*-CPGMA2-*c*-REDV microspheres after 7 days of incubation in cell suspension.

4. Conclusion

Biodegradable PCL microspheres were synthesized by double emulsion solvent extraction/evaporation method, and further grafted with the carboxylated poly(glycidyl methacrylate)-REDV conjugates as favorable microcarriers for the endothelial cell expansion. The PCL microspheres were first activated by aminolysis treatment to introduce an alkyl bromide-containing initiator, followed by grafting of azido-terminated poly(glycidyl methacrylate) (PGMA-N_3) brushes via surface-initiated ATRP. The coupling of reactive carboxyl groups to the pendent azido groups in side chains of PGMA-N_3 brushes were achieved by azide-alkyne click reaction with hexynioc acid. REDV peptides

were finally conjugated to the pendent carboxyl groups on the side chain of carboxylated PGMA-COOH brushes via carbodiimide chemistry to improve cytocompatibility of PCL microspherical scaffolds. ATR-FTIR, XPS, wet laser size analyzer and SEM were used to characterize the synthesis steps, as well as building the final REDV layered coatings. The specificity of cellular interactions of endothelial cells on the REDV-functionalized microsphere surfaces was investigated. *In vitro* cellular studies demonstrated cell adhesion and proliferation of HUVECs were significantly improved on the REDV-immobilized PCL microspheres, and this improvement was positively correlated with the surface density of covalently-conjugated REDV peptides. With versatile and controllable features of surface-initiated ATRP and azide-alkyne click chemistry, the strategy based upon combination of these techniques provides a potentially promising way to decorate a wide variety of biomaterials so as to mimic the characteristics and functions of natural extracellular matrix (ECM) for the manipulation of cells.

Associated content

Supporting Information. The 1H-NMR and FTIR spectra of the synthesized of GMA-N_3 monomer (Figs. S1 and S2), XPS spectra of the pristine PCL and aminolyzed PCL-NH_2 surface from aminolysis treatment (Figs. S3), XPS spectra of the PCL-Br surface (Fig. S4), size distribution curves of the functionalized PCL microsphere (Fig. S5), grafting kinetic curves of PGMA-N_3 brushes as a function of reaction time (Fig. S6), ATR-FTIR spectra of the carboxylated CPGMA-COOH-grafted surfaces (Fig. S7).

Acknowledgment

The authors would like to acknowledge the financial assistance of key project of National Natural Science Foundation of China (NO. 21236004).

Notes and references

1. H. Yu, P. J. VandeVord, W. Gong, B. Wu, Z. Song, H. W. Matthew, P. H. Wooley and S.-Y. Yang, *J. Orthop. Res.* 2008, **26**, 1147-1152.
2. Y. Liu, T. T. Y. Tan, S. J. Yuan and C. Choong, *J. Mater. Chem. B*, 2013, **1**, 157-167.
3. A. Ketchedjian, A. L. Jones, P. Krueger, E. Robinson, K. Crouch, L. Wolfinbarger and R. Hopkins, *Ann. Thorac. Surg.* 2005, **79**, 888-896.
4. G. H. Borschel, Y. C. Huang, S. Calve, E. M. Arruda, J. B. Lynch, D. E. Dow, W. M. Kuzon, R. G. Dennis and D. L. Brown, *Tissue Eng.* 2005, **11**, 778-786.
5. D. T. Simionescu, Q. Lu, Y. Song, J. Lee, T. N. Rosenbalm, C. Kelley and N. R. Vyavahare, *Biomaterials*, 2006, **27**, 702-713.
6. M. A. Cleary, E. Geiger, C. Grady, C. Best, Y. Naito and C. Breuer, *Trends Mol. Medi.* 2012, **18**, 394-404.
7. A. Ratcliffe, *Matrix Biol.* 2000, **19**, 353-357.
8. A. P. McGuigan and M. V. Sefton, *Biomaterials*, 2007, **28**, 2547-2571.
9. A. P. McGuigan and M. V. Sefton, *Biomaterials*, 2008, **29**, 2453-2463.
10. S. Li and J. J. Henry, *Annu. Revi. Biomed. Eng.* 2011, **13**, 451-475.
11. M. S. Hahn, M. K. McHale, E. Wang, R. H. Schmedlen and J. L. West, *Ann. Biomed. Eng.* 2007, **35**, 190-200.
12. S. I. Jeong, J. H. Kwon, J. I. Lim, S. W. Cho, Y. Jung, W. J. Sung, S. H. Kim, Y. H. Kim, Y. M. Lee and B. S. Kim, *Biomaterials*, 2005, **26**, 1405-1411.
13. C. A. Thompson, P. Colon-Hernandez, I. Pomerantseva, B. D. MacNeil, B. Nasseri, J. P. Vacanti and S. N. Oesterle, *Tissue Eng.* 2002, **8**, 1083-1088.
14. T. N. McAllister, M. Maruszewski, S. A. Garrido, W. Wystrychowski, N. Dusserre, A. Marini, K. Zagalski, A. Fiorillo, H. Avila and X. Manglano, *Lancet*, 2009, **373**, 1440-1446.
15. N. L'Heureux, N. Dusserre, G. Konig, B. Victor, P. Keire, T. N. Wight, N. A. Chronos, A. E. Kyles, C. R. Gregory and G. Hoyt, *Nat. Med.* 2006, **12**, 361-365.
16. A. M. Seifalian, A. Tiwari, G. Hamilton and H. J. Salacinski, *Artif. Organs*, 2002, **26**, 307-320.
17. P. Van Hemert, D. Kilburn and A. Van Wezel, *Biotechnol. Bioeng.* 1969, **11**, 875-885.
18. M. Lecina, S. Ting, A. Choo, S. Reuveny and S. Oh, *Tissue Eng. Part C*, 2010, **16**, 1609-1619.
19. S. Hong, H. Yu and H. Kim, *Macromol. Biosci.* 2009, **9**, 639-645.
20. B. Luo, Q. L. Loh, M. T. C. Wong, N. S. Tan and C. Choong, *J. Mater. Chem. B*, 2014, **2**, 7795-7803.
21. Y. Yuan, M. S. Kallos, C. Hunter and A. Sen, *J. Tissue Eng. Regen. M.*. 2014, **8**, 210-225.
22. R. A. Perez, A. El-Fiqi, J. H. Park, T. H. Kim, J. H. Kim and H. W. Kim, *Acta Biomater.* 2014, **10**, 520-530.
23. N. Georgi, C. van Blitterswijk and M. Karperien, *Tissue Engi. Part A*, 2014, **20**, 2513-2523.
24. A. A. Demetriou, J. F. Whiting, D. Feldman, S. M. Levenson, N. R. Chowdhury, A. D. Moscioni and M. Kram, *Science*, 1986, **233**, 1190-1192.
25. X. B. Wu, C.-H. Peng, F. Huang, J. Kuang, S. L. Yu, Y. D. Dong and B. S. Han, *HBPD Int.* 2011, **10**, 509-515.
26. S. Pettersson, J. Wettero, P. Tengvall and G. Kratz, *Biomed. Mater.* 2011, **6**, 065001.
27. Y. Martin, M. Eldardiri, D. J. Lawrence-Watt and J. R. Sharpe, *Tissue Eng. Part B* 2010, **17**, 71-80.
28. S. Stich, Y. Ibold, A. Abbas, M. Ullah, M. Sittinger, J. Ringe, G. Schulze-Tanzil, C. Muller, B. Kohl and T. John, *Biotechnol. Prog.* 2014, **30**, 142-151.
29. R. M. McLoughlin, R. M. Solinga, J. Rich, K. J. Zaleski, J. L. Cocchiaro, A. Risley, A. O. Tzianabos and J. C. Lee, *P. Nat. Acad. Sci.* 2006, **103**, 10408-10413.
30. C. A. Nickerson, T. J. Goodwin, J. Terlonge, C. M. Ott, K. L. Buchanan, W. C. Uicker, K. Emami, C. L. LeBlanc, R. Ramamurthy and M. S. Clarke, *Infect. Immun.* 2001, **69**, 7106-7120.
31. A. Hasan, A. Memic, N. Annabi, M. Hossain, A. Paul, M. R. Dokmeci, F. Dehghani and A. Khademhosseini, *Acta Biomater.* 2014, **10**, 11-25.
32. H. Tseng, D. S. Puperi, E. J. Kim, S. Ayoub, J. V. Shah, M. L. Cuchiara, J. L. West and K. J. Grande-Allen, *Tissue Eng. Part A*, 2014, **20**, 2634-2645.
33. C. Srinivasa Reddy, J. Reddy Venugopal, S. Ramakrishna and E. Zussman, *J. Biomed. Mater. Res. Part A*, 2014, **102**, 3713-3725.
34. N. Thadavirul, P. Pavasant and P. Supaphol, *J. Biomed. Mater. Res. Part A* 2014, **102**, 3379-3392.
35. D. Ishii, T. H. Ying, A. Mahara, S. Murakami, T. Yamaoka, W.-k. Lee and T. Iwata, *Biomacromolecules*, 2008, **10**, 237-242.
36. C. X. Lam, D. W. Hutmacher, J. Schantz, M. A. Woodruff and S. H. Teoh, *J. Biomed. Mater. Res. Part A* 2009, **90**, 906-919.
37. S. A. Abbah, C. X. Lam, D. W. Hutmacher, J. C. Goh and H. K. Wong, *Biomaterials*, 2009, **30**, 5086-5093.
38. G. M. Xiong, S. J. Yuan, C. K. Tan, J. K. Wang, Y. Liu, T. T. Y. Tan, N. S. Tan and C. Choong, *J. Mater. Chem. B*, 2014, **2**, 485-493.
39. S. J. Yuan, G. M. Xiong, A. Roguin and C. Choong, *Biointerphases*, 2012, **7**, 30.
40. Y. Zhu, C. Gao and J. Shen, *Biomaterials*, 2002, **23**, 4889-4895.
41. F. J. Xu, Z. Wang and W. T. Yang, *Biomaterials*, 2010, **31**, 3139-3147.
42. H. Jiang and F. J. Xu, *Chem. Soc. Rev.* 2013, **42**, 3394-3426.
43. Y. Hu, N. Zhao, J. Li, W. Yang and F. Xu, *J. Mater. Chem.* 2012, **22**, 21257-21264.
44. Y. M. Shin, K. S. Kim, Y. M. Lim, Y. C. Nho and H. Shin, *Biomacromolecules*, 2008, **9**, 1772-1781.
45. J. S. Bae, E. J. Seo and I.-K. Kang, *Biomaterials*, 1999, **20**, 529-537.
46. S. J. Yuan and S. O. Pehkonen, *Colloid Surface B* 2007, **59**, 87-99.
47. Y. Y. Yang, T. S. Chung and N. P. Ng, *Biomaterials*, 2001, **22**, 231-241.
48. S. Jameela, N. Suma and A. Jayakrishnan, *J. Biomat. Sci. Polym. E.* 1997, **8**, 457-466.

49. F. Causa, E. Battista, R. Della Moglie, D. Guarnieri, M. Iannone and P. A. Netti, *Langmuir*, 2010, **26**, 9875-9884.
50. H. Zhang, C. Y. Lin and S. J. Hollister, *Biomaterials*, 2009, **30**, 4063-4069.
51. L. Zhao, Y. H. Xu, T. Akasaka, S. Abe, N. Komatsu, F. Watari and X. Chen, *Biomaterials*, 2014, **35**, 5393-5406.
52. J. F. Moulder, J. Chastain and R. C. King, *Handbook of X-ray photoelectron spectroscopy*. Perkin-Elmer Eden Prairie, MN, 1992.
53. S. J. Yuan, G. M. Xiong, X. Y. Wang, S. Zhang and C. Choong, *J. Mater. Chem.*, 2012, **22**, 13039-13049.
54. K. Matyjaszewski and J. Xia, *Chem. Rev.* 2001, **101**, 2921-2990.
55. E. Soto-Cantu, B. S. Lokitz, J. P. Hinestrosa, C. Deodhar, J. M. Messman, J. F. Ankner and S. M. Kilbey II, *Langmuir*, 2011, **27**, 5986-5996.
56. P. Pandey, O. K. Farha, A. M. Spokoyny, C. A. Mirkin, M. G. Kanatzidis, J. T. Hupp and S. T. Nguyen, *J. Mater. Chem.* 2011, **21**, 1700.
57. S. Ciampi, T. Bocking, K. A. Kilian, M. James, J. B. Harper and J. J. Gooding, *Langmuir*, 2007, **23**, 9320-9329.
58. J. A. Hubbell, S. P. Massia, N. P. Desai and P. D. Drumheller, *Nat. Biotechnol.* 1991, **9**, 568-572.
59. A. Mahara, S. Somekawa, N. Kobayashi, Y. Hirano, Y. Kimura, T. Fujisato and T. Yamaoka, *Biomaterials*, 2015, **58**, 54-62.
60. Q. K. Lin, Y. Hou, K. F. Ren and J. Ji, *Thin Solid Films*, 2012, **520**, 4971-4978.
61. Q. Ji, S. Zhang, J. Zhang, Z. Wang, J. Wang, Y. Cui, L. Pang, S. Wang, D. Kong and Q. Zhao, *Biomacromolecules*, 2013, **14**, 4099-4107.
62. X. Ren, Y. Feng, J. Guo, H. Wang, Q. Li, J. Yang, X. Hao, J. Lv, N. Ma and W. Li, *Chem. Soc. Rev.* 2015, in press
63. L. Zhang, H. Xue, C. Gao, L. Carr, J. Wang, B. Chu and S. Jiang, *Biomaterials*, 2010, **31**, 6582-6588.
64. H. Wang, Y. Feng, J. Yang, J. Guo and W. Zhang, *J. Mater. Chem. B*, 2015, **3**, 3379-3391.
65. Y. Zhu, C. Gao, X. Liu and J. Shen, *Biomacromolecules*, 2002, **3**, 1312-1319.
66. U. Aydemir Sezer, D. Arslantunali, E. A. Aksoy, V. Hasirci and N. Hasirci, *J. Appl. Polym. Sci.* 2014, **131**, 40110
67. G. Z. Jin, J. H. Park, E. J. Lee, I. B. Wall and H. W. Kim, *Tissue Eng. Part C*, 2014, **20**, 761-768.
68. P. Van Wachem, T. Beugeling, J. Feijen, A. Bantjes, J. Detmers and W. Van Aken, *Biomaterials*, 1985, **6**, 403-408.
69. N. Faucheux, R. Schweiss, K. Lutzow, C. Werner and T. Groth, *Biomaterials*, 2004, **25**, 2721-2730.

TOC Graphic

Title: PCL microspheres tailored with carboxylated poly(glycidyl methacrylate)-REDV conjugates as conducive microcarriers for endothelial cell expansion

Authors: Shaojun Yuan,[a,*] Gordon Xiong,[b,] Fei He,[a] Wei Jiang,[a] Bin Liang,[a] Simo Pehkonen,[c] Cleo Choong[b,*]

TOC Graphic: